

Platypose: Calibrated Zero-Shot Multi-Hypothesis 3D Human Motion Estimation

Paweł A. Pierzchlewicz^{1,2} , Caio da Silva² ,
R. James Cotton^{3,4} , and Fabian H. Sinz^{1,2,5,6} 

¹ Institute for Bioinformatics and Medical Informatics, Tübingen University,
Tübingen, Germany

² Department of Computer Science and Campus Institute Data Science (CIDAS),
Göttingen University, Göttingen, Germany

³ Shirley Ryan AbilityLab, Chicago, IL, USA

⁴ Department of Physical Medicine and Rehabilitation, Northwestern University,
Evanston, IL, USA

⁵ Department of Neuroscience, Baylor College of Medicine, Houston, TX, USA

⁶ Center for Neuroscience and Artificial Intelligence, Baylor College of Medicine,
Houston, TX, USA

ppierzcz@cs.uni-goettingen.de

Abstract. Single camera 3D pose estimation is an ill-defined problem due to inherent ambiguities from depth, occlusion or keypoint noise. Multi-hypothesis pose estimation accounts for this uncertainty by providing multiple 3D poses consistent with the 2D measurements. Current research has predominantly concentrated on generating multiple hypotheses for single frame static pose estimation. In this study we focus on the new task of multi-hypothesis motion estimation. Motion estimation is not simply pose estimation applied to multiple frames, which would ignore temporal correlation across frames. Instead, it requires distributions which are capable of generating temporally consistent samples, which is significantly more challenging. To this end, we introduce Platypose, a framework that uses a diffusion model pretrained on 3D human motion sequences for zero-shot 3D pose sequence estimation. Platypose outperforms baseline methods on multiple hypotheses for motion estimation. Additionally, Platypose also achieves state-of-the-art calibration and competitive joint error when tested on static poses from Human3.6M, MPI-INF-3DHP and 3DPW. Finally, because it is zero-shot, our method generalizes flexibly to different settings such as multi-camera inference.

Keywords: Motion Estimation · Diffusion Models · Zero-Shot · Calibrated Uncertainty

1 Introduction

Estimating 3D human motions holds paramount significance across various domains such as gait analysis [46], sports analytics [2, 19], and character anima-

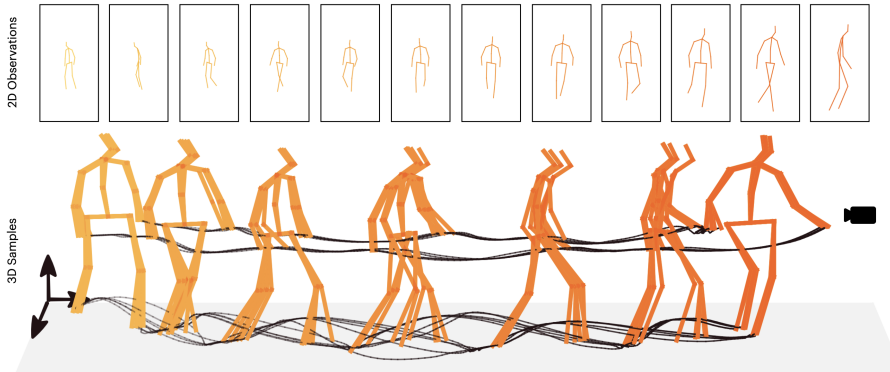


Fig. 1: Example samples from the posterior, Platypose generates samples with smooth motion. Darker color indicates later frames in time. Trajectories of wrists and feet are shown for each frame. Top 5 samples are shown at frames 64, 96, 128, 192, 224, 255. Camera icon indicates the direction from which the 2D observations are obtained.

tion [25, 47]. In these contexts, motion plays a pivotal role as these applications rely heavily on temporal dynamics.

Motion estimation involves predicting a consistent sequence of poses based on 2D observations, as opposed to **pose estimation** which estimates a static pose for a single frame. Despite some methodologies delving into motion estimation [42, 50, 51], a significant challenge persists: current approaches typically provide only a single plausible sequence, thereby neglecting the inherent ambiguity in motion estimation. This ambiguity arises from factors such as depth, occlusion, and noise in 2D keypoint detection. However, multi-hypothesis motion estimation remains an unexplored, thus the problem of ambiguity remains unresolved.

Incorporating uncertainties into estimates offers valuable insights for users: Medical practitioners, for instance, can benefit from a more transparent and dependable system that alerts them to areas of uncertainty. Character animators gain a wider range of plausible 3D motions, enhancing their ability to express their artistic vision. These benefits are not available with the single-hypothesis solutions. However, estimating multiple hypotheses for *motion* presents a significant challenge compared to multi-hypothesis *pose* estimation (figure 2). Unlike the latter, motion estimation requires temporal consistency, thus increasing the complexity of sampling plausible sequences beyond simply sampling static poses for each individual frame. Furthermore, many existing multi-hypothesis pose estimation methods suffer from miscalibration, rendering their uncertainty estimates uninformative as they fail to capture the underlying ambiguities of the problem [34].

To address these challenges, we introduce Platypose, a zero-shot motion estimation framework. Platypose can infer 3D motion sequences from 2D observations (figure 1) without requiring explicit training on 2D-3D pairs, thanks to

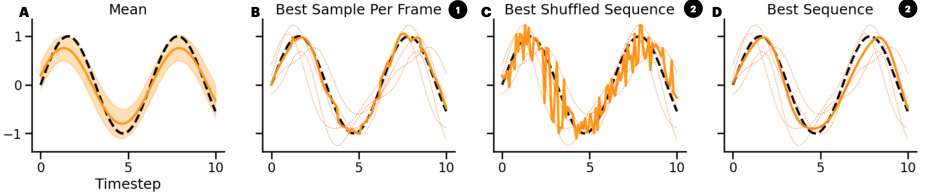


Fig. 2: Simplified sequence estimation problem. **A)** Mean and standard deviation of a Gaussian process fit to a sine function. **B)** Result of strategy 1 – choosing the best sample in each frame – same for both shuffled and non shuffled sequences. **C)** Result for strategy 2 – best sequence fit as a whole – for the shuffled sequences. **D)** Result for strategy 2 – best sequence fit as a whole – for the sequences sampled from the Gaussian process. Dotted lines are the samples from the Gaussian process, solid line is the selected sequence. Dashed line is the ground truth sine wave.

pretraining a motion diffusion model [44] and using energy guidance [35]. Our key contributions are the following:

- We propose a zero-shot motion estimation framework, which uses a pre-trained 3D motion diffusion model to synthesize 3D motions conditioned on 2D observations using energy guidance.
- We achieve a 10x reduction in inference time through the generation of samples in just 8 steps.
- We demonstrate state-of-the-art performance in multi-hypothesis motion estimation, alongside achieving state-of-the-art calibration for pose estimation.

2 Problem Setting

Estimating multiple hypotheses for motion sequences presents a novel challenge for human behaviour analysis. The primary goal is to infer the posterior distribution $p(\mathbf{x} | \mathbf{y})$ where \mathbf{x} represents 3D motion sequences and \mathbf{y} denotes 2D observations of these motions. Multi-hypotheses motion estimation comes with two central challenges: **i** Motion estimation entails a significantly higher dimensionality compared to pose estimation. In pose estimation, $\mathbf{x} \in \mathbb{R}^{J \times 3}$, where J is the number of joints. For motion estimation \mathbf{x} expands to $\mathbb{R}^{F \times J \times 3}$, where F represents the number of frames. **ii** Unlike single-hypothesis motion estimation, which predicts a single point estimate such as the mean of the posterior $p(\mathbf{x} | \mathbf{y})$, multi-hypothesis motion estimation needs to capture the complex temporal covariance structure. Consequently, each sample drawn from the distribution should be a valid motion sequence. Simply sampling independent poses for each frame overlooks this problem, resulting in an unrealistically noisy motion sequence. We illustrate this disparity in a simplified scenario (also see figure 2).

Consider the task of estimating a sine function from noisy observation $f(x) = \sin(x) + \varepsilon$, $\varepsilon \sim \mathcal{N}(0, 0.05)$ (see figure 2). We employ a Gaussian Process with an exponential sine squared kernel fitted to the noisy observations. We consider

sequences sampled from the Gaussian process and sequences where samples are shuffled within each frame, effectively removing temporal correlations. We consider 2 evaluation strategies. ① choosing the best sample independently for each frame and ② choosing the best sequence as a whole. Strategy ① corresponds to pose estimation, while strategy ② corresponds to motion estimation. For strategy ① both non-shuffled and shuffled sequences result in the same outcome, as temporal correlations are not relevant for this strategy. This observation demonstrates that even when sequence estimates are suboptimal, the per-frame metrics yield low errors. However, for strategy ② the best shuffled sequence performs significantly worse than the best non-shuffled sequence. This simple example demonstrates that even a subpar sequence model can achieve low errors in pose estimation, while motion estimation necessitates a good sequence model capable of sampling consistent – temporally correlated – sequences.

3 Related Work

Multi-hypothesis Learning Based Lifting Pose estimation can be approached through either image-to-3D or 2D-to-3D methodologies, the latter is commonly referred to as *lifting*. [29] introduced lifting as a *learning-based* task which learns the mapping between 2D and 3D keypoints via a linear ResNet model to transform 2D poses into 3D representations, which outperformed image-to-3D models at that time. Since then, motion based single-hypothesis methods like PoseFormer [50] MotionBERT [51] or MotionAGFormer [42] have been dominant. They use transformer based architectures to predict single sequences of poses from 2D observations. However, the 2D-to-3D lifting task presents an inherent challenge as an ill-posed problem. To address this challenge several multi-hypothesis learning based approaches have been proposed. [26] and [32] propose the use of mixture density networks to capture the distribution of plausible poses. Meanwhile, [38] leverage a variational autoencoder to sample plausible poses and employ ordinal ranking to resolve depth ambiguity. Furthermore, [24], [48], and [34] use normalizing flows to model the inverse nature of lifting. Recent advancements employ a diffusion model conditioned on 2D observations [5, 9, 16]. The methods above are learning-based methods, thus they require training on 2D-to-3D pairs, which is different from Platypose which is never trained on 2D-to-3D pairs.

Zero-Shot Lifting with Diffusion Models Diffusion models are a family of generative models designed to invert a diffusion process, by iteratively removing noise [14, 39]. They are capable of sampling from complex distributions, including images [6, 14], videos [1, 15] or human motions [36, 44] proving highly effective in the realm of human pose estimation [5, 9, 16]. Moreover, diffusion models have found application in *zero-shot* pose estimation. ZeDO [20] employs a score-based diffusion model with an optimizer in the loop to achieve zero-shot pose estimation. Initially, a pose is optimized by sampling from the training set and refining its rotation and translation. Subsequently, this initialized pose undergoes

processing via a score-based diffusion model, with an optimizer in the loop to minimize the reprojection error over 1000 steps. Similarly, PADS [18] adopts a comparable strategy to ZeDO, albeit with a distinction in the initialization of the pose. They further find that the optimization process can be truncated to 450 steps, thus improving sampling speed. The above methods differ from Platypose, which 1) is designed for *motion* estimation, 2) predicts the denoised sample directly, allowing sample generation in 8 steps, which dramatically decreases inference time and 3) ZeDO and PADS use pose initialization, which Platypose does not.

Human Motion Synthesis The synthesis of human motion sequences has garnered significant attention in the recent years. Now these methods allow high fidelity modeling of the distributions of 3D motions. Advancements in text-to-motion synthesis have showcased remarkable progress. [13] propose a Variational Autoencoder (VAE) mapping text embeddings to a Gaussian distribution in the latent space. [43] expand the text-image embedding space of CLIP [37] to include motion representations. Building on this, [44] have proposed a motion diffusion model (MDM), which is a transformer-based diffusion model that learns the posterior distribution of 3D motions given text descriptions. Recently, [12] propose a motion residual vector quantized VAE achieving the current state-of-the-art performance in motion synthesis.

Calibration poses a significant challenge in multi-hypothesis pose estimation, an issue that has been explored in recent studies [11, 34]. [34] highlighted that multi-hypothesis pose estimation methods often suffer from significant miscalibration. They show that miscalibration tends to erroneously reduce joint errors by underestimating the uncertainty. Consequently, such miscalibrated methods prove ineffective to provide insight into the underlying ambiguities in real-world scenarios.

4 Method

4.1 Lifting as Zero-Shot Sampling

Our goal is to generate samples from a posterior $p(\mathbf{x} \mid \mathbf{y})$ given a prior $p(\mathbf{x})$ and a likelihood $p(\mathbf{y} \mid \mathbf{x})$ where $\mathbf{x} \in \mathbb{R}^{F \times J \times 3}$ are the 3D motion sequences and $\mathbf{y} \in \mathbb{R}^{F \times J \times 2}$ are the 2D observations in camera frames. We model the prior $p(\mathbf{x})$ as a single-step diffusion model [14], which shares similarities with a consistency model [40]. Initially, a standard diffusion model adds noise to the data employing a forward stochastic differential equation

$$d\mathbf{x}_t = \mu(\mathbf{x}_t, t)dt + \sigma(t)d\mathbf{w}, \quad (1)$$

where $t \in [0, T]$ is the diffusion timestep, μ and σ are the drift and diffusion coefficients and \mathbf{w} denotes the Wiener process. Subsequently, the diffusion model then denoises the data by following the probability flow ODE [41]:

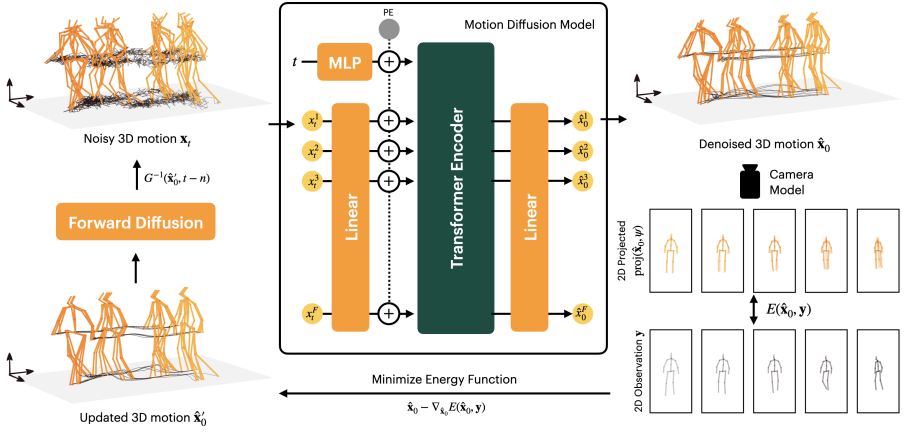


Fig. 3: Schematic of sampling using Platypose – A noisy 3D motion \mathbf{x} is denoised by a motion diffusion model trained on H36M. The denoised 3D motion samples $\hat{\mathbf{x}}_0$ are projected to 2D with a camera model. The reprojection error between the projections and 2D observations is minimized. The updated 3D motion is diffused to $t - n$ and passed back into the diffusion model.

$$g(\mathbf{x}_t, t) = \frac{d\mathbf{x}}{dt} = \mu(\mathbf{x}_t, t) - \frac{1}{2} \sigma(t)^2 \nabla_{\mathbf{x}_t} \log p_t(\mathbf{x}_t) \quad (2)$$

Samples \mathbf{x}_0 from the prior $p(\mathbf{x})$ can be obtained by integrating $g(\mathbf{x}_t, t)$ from timestep t to 0 with the initial state \mathbf{x}_t .

$$\mathbf{x}_0 = \mathbf{x}_t + \int_t^0 g(\mathbf{x}_\tau, \tau) d\tau = G(\mathbf{x}_t, t) \quad (3)$$

To obtain a single-step diffusion model, similar to [14, 40, 44], we model the de-

Algorithm 1 Sampling

Require: \mathbf{y} 2D pose measurement, \mathbf{c} observation confidence, T total diffusion timesteps, S skip timesteps, n respace step size, λ energy scale, θ model parameters

Sample $\mathbf{x}_{init} \sim \mathcal{N}(\mathbf{0}, \mathbf{I})$

$$\mathbf{x}_{T-S} \leftarrow G^{-1}(\mathbf{x}_{init}, T - S)$$

for $t \leftarrow T - S$ to 0 **do**

$$\hat{\mathbf{x}}_0 \leftarrow G_\theta(\mathbf{x}_t, t)$$

for k iterations **do**

$$\hat{\mathbf{x}}_0 \leftarrow \hat{\mathbf{x}}_0 - \mathbf{c} \lambda \nabla_{\hat{\mathbf{x}}_0} E(\hat{\mathbf{x}}_0, \mathbf{y})$$

end for

$$\mathbf{x}_{t-n} \leftarrow G^{-1}(\hat{\mathbf{x}}_0, t - n)$$

end for

return \mathbf{x}_0

noiser $G_\theta(\mathbf{x}, t)$ as a deep neural neural network model with parameters θ . Unlike conventional score-based diffusion models, which estimate the score $\nabla_{\mathbf{x}_t} \log p_t(\mathbf{x}_t)$ at each timestep, our denoiser directly predicts the denoised sample \mathbf{x}_0 (see model details in Sec. 4.2). However, for zero-shot conditioning, we need a multi-step generation procedure. To obtain an intermediate step \mathbf{x}_t we run the forward diffusion process $G^{-1}(\mathbf{x}_0, t) = \sqrt{\bar{\alpha}_t} \mathbf{x}_0 + \sqrt{1 - \bar{\alpha}_t}$, where $\bar{\alpha}_t = \prod_{i=0}^t 1 - \sigma(i)$. This yields a multi-step sampling process with a respacing step size n .

$$\mathbf{x}_{t-n} = G^{-1}(G_\theta(\mathbf{x}_t, t), t - n) \quad (4)$$

We find it optimal to respace the sampling process to 8 steps from 50 (see Sec. 5.4). To acquire samples from the posterior distribution we guide the diffusion process using energy guidance [35] (Fig. 3). We choose the likelihood to be a Normal distribution around the reprojected 3D keypoints in the image $p(\mathbf{y} | \mathbf{x}) = \mathcal{N}(\mathbf{y}; \text{proj}(\mathbf{x}_0, \vartheta), \lambda^{-1} \mathbf{I})$ for which the energy function corresponds to the reprojection error

$$E(\mathbf{x}_0, \mathbf{y}) = \log p(\mathbf{y} | \mathbf{x}) = \lambda \cdot \|\mathbf{y} - \text{proj}(\mathbf{x}_0, \vartheta)\|_2^2. \quad (5)$$

Here, ϑ represents camera parameters, \mathbf{y} denotes 2D observations and λ is the energy scale or precision. Note that the energy is defined for \mathbf{x}_0 but not for intermediate \mathbf{x}_t at different steps in the diffusion sampling process. However, since we use a one-step diffusion $\hat{\mathbf{x}}_0 = G_\theta(\mathbf{x}_t, t)$, we approximate \mathbf{x}_0 for the energy with $G_\theta(\mathbf{x}_t, t)$. We integrate energy guidance into equation 4.

$$\hat{\mathbf{x}}_0 = G_\theta(\mathbf{x}_t, t) \quad (6)$$

$$\hat{\mathbf{x}}'_0 = \hat{\mathbf{x}}_0 - \lambda \nabla_{\hat{\mathbf{x}}_0} E(\hat{\mathbf{x}}_0, \mathbf{y}) \quad (7)$$

$$\mathbf{x}_{t-n} = G^{-1}(\hat{\mathbf{x}}'_0, t - n) \quad (8)$$

We find empirically that performing the update step (equation 7) multiple times improves performance. Performing k update steps can be interpreted as evaluating the dynamics of the sample using a k -th order Yoshida integrator [49]. We also find that skipping the first S diffusion timesteps improves calibration. The full sampling procedure is defined in Algorithm 1.

4.2 Motion Diffusion Prior

We base our motion diffusion prior on the unconstrained motion diffusion model [44], illustrated in Fig. 3. The model G_θ is implemented as an encoder-only transformer model [45]. The diffusion timestep t is first positionally encoded and then projected into 512 dimensions with 2 linear layers with a SiLU activation function [7] constructing an input token. Each frame f of the noisy motion sequence $\mathbf{x}_t^f \in \mathbb{R}^{J \times 3}$ is linearly projected into 512 dimensions and added to standard positional embedding [45]. Each frame serves as a separate input token for the transformer. Finally, all output tokens, except the first, are linearly decoded into the pose dimension.

Training The diffusion model is trained with the objective to predict the denoised sequence \mathbf{x}_0 directly.

$$\mathcal{L}(\theta) = \mathbb{E}_{\mathbf{x}_0 \sim \mathcal{D}, t \sim [1, T]} \|G_\theta(\mathbf{x}_t, t) - \mathbf{x}_0\|_2^2 \quad (9)$$

The diffusion model is trained with $T = 50$ timesteps. In each training iteration we sample a sequence length from a uniform distribution $\mathcal{U}(1, F)$, where F is the max sequence length. The training process is described by Algorithm 2.

Algorithm 2 Training

Require: \mathcal{D} dataset of 3D motions, initial model parameters θ , learning rate η

repeat

 Sample $\mathbf{x}_0 \sim \mathcal{D}$, and $t \sim \mathcal{U}(1, T)$, and $f \sim \mathcal{U}(1, F)$.

$\mathbf{x}_t \leftarrow G^{-1}(\mathbf{x}_0^{0:f}, t)$

$\mathcal{L}(\theta) \leftarrow \|G_\theta(\mathbf{x}_t, t) - \mathbf{x}_0^{0:f}\|_2^2$

$\theta \leftarrow \theta - \eta \nabla_\theta \mathcal{L}(\theta)$

until convergence

4.3 2D Observation Confidences

Platypose can integrate 2D observation confidences \mathbf{c} into its sampling process. This is achieved by scaling the gradient of the energy by \mathbf{c} . Equation 5 assumes an isotropic Gaussian likelihood for the reprojected keypoints. Scaling the energy by \mathbf{c} is equivalent to changing the precision of this likelihood

$$E(\mathbf{x}_0, \mathbf{y}) \sim \log \mathcal{N}(\mathbf{y}; \text{proj}(\mathbf{x}_0, \vartheta), \mathbf{c}^{-1} \lambda^{-1} \mathbf{I}) \quad (10)$$

To estimate post-hoc confidences, we propose a proxy using ground truth 2D observations \mathbf{y}^* . Here, we define the confidences as $\mathbf{c} = |\mathbf{y}^* - \text{proj}(\mathbf{x}_0, \vartheta)|$. When using ground truth keypoints we set $\mathbf{c} = \mathbf{I}$. We explore the performance implications of including confidences in Sec. 5.4.

4.4 Energy Scale Decay

The energy scale λ controls the default variance of the likelihood. However, relying solely on a singular value of λ proves inadequate for optimal performance across all scenarios because the variance in 2D observations exhibits a dependency on depth: poses situated farther from the camera yield less variance in 2D compared to those in closer proximity. To address this inherent variability systematically, we introduce an energy scale decay mechanism. This decay process involves a reduction in the energy scale by a factor of 0.1 whenever the energy $E(\mathbf{x}_0, \mathbf{y})$ increases between consecutive update steps (equation 7).

5 Experiments

In this section we introduce experimental results for Platypose on Human3.6M, MPI-INF-3DHP and 3DPW. We first show the results of Platypose on motion estimation in comparison to a baseline method. Since baselines in this domain do not exist we construct a baseline by adding a Gaussian distribution to the mean prediction of MotionBERT [51]. Platypose can also predict single frames, therefore, we show a comparison to other single-frame methods.

5.1 Datasets and Metrics

Human3.6M [3, 17] (H36M) The Human3.6M (H36M) dataset comprises 3.6 million frames from four cameras and corresponding 3D poses obtained via high-speed motion capture. It features 11 actors (6 males, 5 females) across 17 scenarios. For training, we use subjects S1, 5, 6, 7, and 8, with evaluation conducted on subjects S9 and S11.

MPI-INF-3DHP [30] (3DHP) is a single-person 3D pose dataset with 1.3 million frames captured in indoor, green screen and outdoor settings, involving 8 actors (4 males, 4 females). The dataset includes diverse actions ranging from simple to dynamic movements such as exercises. Evaluation is performed on the 6 test sequences defined in the dataset, using the 17 H36M keypoints.

3D Poses in the Wild [28] (3DPW) focuses on in-the-wild human poses captured with moving cameras, comprising 60 videos of 18 actors. We evaluate on the test set of the 3DPW dataset and use the 17 H36M keypoints.

Evaluation Metrics We report values in four metrics. Firstly, minimum mean per joint position error (minMPJPE), measures the mean Euclidean distance between each joint of a pose, with the best hypothesis value reported. Next, we calculate the mean per joint velocity error (MPJVE), representing the L2 error of joint velocities, based on the sequence that minimizes minMPJPE. We also report the Procrustes-aligned mean per joint position error (PA-MPJPE), which applies rigid alignment post-processing to the predicted poses before computing minMPJPE. Finally, we asses the expected calibration error (ECE) as defined in [34]. ECE is expressed as $ECE = |q - \omega(q)|$, where $q \in [0, 1]$ denotes quantiles and $\omega(q)$ represents the frequencies with which ground truth 3D keypoints fall into the predicted distribution's given quantile.

5.2 Training and Inference Details

The diffusion prior was trained for 600,000 steps using the AdamW [27] optimizer with a learning rate of 10^{-4} and batch size of 64. Training was executed on a single GeForce 2080Ti GPU in 25 hours. The model was trained only on the

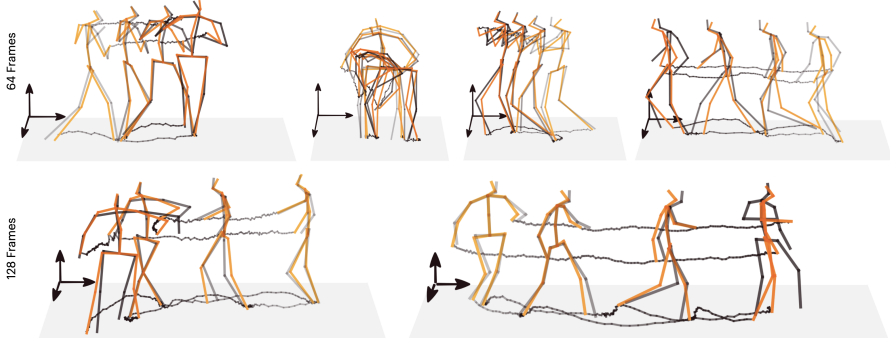


Fig. 4: Examples of 3D motion estimates for Human3.6M. Darker color indicates later frames in time. Trajectories of wrists and feet are shown for each frame. Orange poses represent the best sampled hypothesis out of 200 samples, black poses are the ground truth 3D poses.

train set of Human3.6M with a max sequence length of $F = 256$ and $T = 50$ diffusion timesteps. The pretrained models and code for training and evaluation are available at <https://github.com/sinzlab/platopose>.

5.3 Results

Motion Estimation Baseline Given the absence of prior work on estimating multiple hypotheses for motion sequences, we establish our own baseline. We use the off-the-shelf MotionBERT model [51], which is a learning based model for single-hypothesis motion estimation achieving 37.5 mm MPJPE error with predicted 2D keypoints. Inspired by [34] we develop a multi-hypothesis motion estimation variant of the MotionBERT. We define the posterior as a Gaussian distribution.

$$p(\mathbf{x} \mid \mathbf{y}) = \mathcal{N}(\mathbf{x}; \mu(\mathbf{y}), \sigma^2 \mathbf{I}) \quad (11)$$

where $\mu(\mathbf{y})$ is the output of the MotionBERT model. The variance σ^2 is learned to maximize the log likelihood of the posterior $\arg \max_{\sigma} p(\mathbf{x}^* \mid \mathbf{y})$. The baseline corresponds to the shuffled sequences introduced in Sec. 2

Motion estimation on H36M We evaluate the generation of multiple hypotheses for sequences of different lengths (16, 64 and 128 frames) using the H36M dataset (Tab. 1). We use $T = 10$, $S = 2$, $\lambda = 30$. We show examples of the best hypotheses from Platopose in figure 4. Additional examples can be found in the supplementary materials. Our baseline model, MotionBERT, reveals that merely adding Gaussian noise to a solid mean estimate is not adequate for achieving high-quality, temporally-consistent, multi-hypothesis sequence estimates. We demonstrate that Platopose surpasses MotionBERT in terms of minMPJPE and PA-MPJPE, while also significantly outperforming MotionBERT in MPJVE.

The baseline shows lower ECE, which is expected as the variance was explicitly trained for uncertainty quantification. In summary, Platypose offers the best of both worlds: superior MPJVE and a low minMPJPE.

| Method | Frames | minMPJPE ↓ | PA-MPJPE ↓ | MPJVE ↓ | ECE ↓ |
|-----------------|--------|-------------|-------------|-------------|-------------|
| MotionBERT [51] | 16 | 57.8 | 51.0 | 54.8 | 0.03 |
| | 64 | 56.4 | 50.4 | 56.0 | 0.03 |
| | 128 | 56.3 | 50.4 | 56.4 | 0.04 |
| Platypose | 16 | 47.8 | 38.5 | 9.58 | 0.09 |
| | 64 | 53.9 | 43.1 | 9.67 | 0.09 |
| | 128 | 60.0 | 47.7 | 9.72 | 0.09 |

Table 1: Human3.6M motion estimation results, CPN Keypoints, 200 samples, **bold** indicates best for each number of frames.

Multi-Camera Motion Estimation Platypose can naturally scale to multiple cameras without any additional training. By simply modifying the energy function, the model can effectively handle data from multiple viewpoints. The energy function with observations from N cameras is defined as:

$$E(\mathbf{x}, \mathbf{y}) = \sum_i^N \|\mathbf{y}_i - \text{proj}(\mathbf{x}, \vartheta_i)\|_2^2 \quad (12)$$

The results presented in Tab. 2 showcase Platypose’s performance across varying numbers of cameras (2-4) on the H36M dataset. Joint errors decrease as the number of cameras increases, yet the distribution tends to become miscalibrated. This phenomenon is likely attributed to the increasing rigidity imposed by the constraints from multiple cameras, leading to overconfident estimates of the 3D poses. These results showcase that the zero-shot nature of Platypose allows seamless integration of data from multiple sources.

| Cameras | Frames | minMPJPE ↓ | PA-MPJPE ↓ | MPJVE ↓ | ECE ↓ |
|---------|--------|------------|------------|---------|-------|
| 2 | 16 | 13.6 | 11.4 | 2.17 | 0.12 |
| | 3 | 7.5 | 6.4 | 1.19 | 0.20 |
| | 4 | 4.7 | 4.1 | 0.79 | 0.29 |
| 2 | 64 | 14.5 | 12.3 | 2.57 | 0.17 |
| | 3 | 8.0 | 6.9 | 1.38 | 0.24 |
| | 4 | 4.8 | 4.3 | 0.75 | 0.34 |
| 2 | 128 | 16.5 | 14.2 | 2.72 | 0.20 |
| | 3 | 9.3 | 8.2 | 1.36 | 0.28 |
| | 4 | 4.8 | 4.4 | 0.69 | 0.35 |

Table 2: Multi-camera motion estimation results, GT Keypoints, 200 samples.

Pose Estimation on H36M We evaluate Platypose on the multi-hypothesis pose estimation task. We use $\lambda = 30$ and $T = 12$, $S = 4$ (*8 Steps*) or $T = 20$, $S = 4$ (*16 steps*). We consider the standard predicted 2D keypoints from the off-the-shelf cascading pyramid network (CPN) model (CPN, Tab. 3). Platypose achieves comparable results to ZeDO on 50 samples and significantly outperforms ZeDO on 200 samples. Additionally, Platypose exhibits superior calibration compared to ZeDO. Furthermore, Platypose surpasses other zero-shot methods and narrows the performance gap between learned methods on predicted keypoints. Moreover, Platypose demonstrates state-of-the-art calibration. Thus, showing that even though Platypose was designed to estimate motion it also is capable at pose estimation.

| Methods | ZS | N | minMPJPE \downarrow | PA-MPJPE \downarrow | ECE \downarrow |
|----------------------------------|----|-----|-----------------------|-----------------------|------------------|
| Sharma et al. (2019) [38] | | 200 | 46.7 | 37.3 | 0.36 |
| Oikarinen et al. (2020) [33] | | 200 | 46.2 | 36.3 | 0.16 |
| Wehrbein et al. (2021) [48] | | 200 | 44.3 | 32.4 | 0.18 |
| Pierzchlewicz et al. (2022) [34] | | 200 | 53.0 | 40.7 | 0.08 |
| Holmquist et al. (2022) [16] | | 200 | <u>42.9</u> | <u>32.4</u> | 0.27 |
| GFPose (2023) [5] | | 200 | 35.6 | 30.5 | <u>0.10</u> |
| ZeDO (2023) [20] | ✓ | 50 | 51.4 | 42.1 | 0.25 |
| PADS (2024) [18] | ✓ | 1 | 54.8 | 44.9 | n/a |
| Platypose (8 steps) | ✓ | 50 | 51.8 | 41.5 | <u>0.03</u> |
| Platypose (8 steps) | ✓ | 200 | 45.6 | 36.9 | 0.02 |
| Platypose (16 steps) | ✓ | 50 | <u>50.9</u> | <u>40.7</u> | 0.04 |
| Platypose (16 steps) | ✓ | 200 | 45.0 | 36.3 | <u>0.03</u> |

Table 3: Human3.6M pose estimation Results, CPN Keypoints, **bold** is best, underline is second best. The best values are considered separately for zero-shot and learning based methods. ZS are zero-shot methods. N – number of hypotheses.

Cross-Dataset Pose Estimation In this section, we assess Platypose’s ability to generalize across datasets, as shown in Tabs. 4 and 5. Using our pretrained diffusion prior from the H36M dataset, we evaluate Platypose’s performance on both the 3DHP and 3DPW test sets. We use $\lambda = 10$ and $T = 12$, $S = 4$ (*8 Steps*) or $T = 20$, $S = 4$ (*16 steps*). Our analysis reveals that Platypose exhibits better calibration compared to alternative methods. Platypose performs well on the 3DPW dataset, where it outperforms previous zero-shot and learned methods in both minMPJPE and PA-MPJPE metrics. This highlights Platypose’s robustness and adaptability across diverse datasets, indicating its potential for real-world applications.

Inference Speed Comparison When testing against ZeDO on a GeForce 2080 Ti we find that Platypose generates a sample 10x faster than ZeDO. This provides a significant boost in performance allowing real-time generation of samples using Platypose.

| Methods | N | MPJPE ↓ | ECE ↓ |
|----------------------------|-----|-------------|-------------|
| Kanazawa et al. [21] | 1 | 113.2 | n/a |
| Gong et al. [10] | 1 | 73.0 | n/a |
| Gholami et al. [8] | 1 | 68.3 | n/a |
| Chai et al. [4] | 1 | 61.3 | n/a |
| Muller et al.† [31] | 1 | 101.2 | n/a |
| ZeDO† [20] | 50 | 69.9 | 0.28 |
| Platypose† (8 St.) | 50 | 74.6 | <u>0.08</u> |
| Platypose† (8 St.) | 200 | <u>64.2</u> | 0.07 |
| Platypose† (16 St.) | 50 | 74.7 | 0.08 |
| Platypose† (16 St.) | 200 | 64.4 | 0.08 |

Table 4: 3DHP Results, GT Keypoints, **bold** is best, underline is second best, † are zero-shot methods. N – number of hypotheses. *St.* stands for Steps.

| Methods | N | MPJPE ↓ | PMPJPE ↓ | ECE ↓ |
|----------------------------|-----|-------------|-------------|-------------|
| Kocabas et al. [22] | 1 | 93.5 | 56.5 | n/a |
| Kocabas et al. [23] | 1 | 82.0 | 50.9 | n/a |
| Gong et al. [10] | 1 | 94.1 | 58.5 | n/a |
| Gholami et al. [8] | 1 | 81.2 | 46.5 | n/a |
| Chai et al. [4] | 1 | 87.7 | 55.3 | n/a |
| ZeDO† [20] | 1 | 69.7 | 40.3 | n/a |
| Platypose† (8 St.) | 50 | 60.1 | 39.6 | <u>0.05</u> |
| Platypose† (8 St.) | 200 | <u>50.6</u> | <u>34.2</u> | 0.04 |
| Platypose† (16 St.) | 50 | 60.2 | 38.7 | 0.06 |
| Platypose† (16 St.) | 200 | 50.8 | 33.9 | 0.05 |

Table 5: 3DPW Results, GT Keypoints, **bold** is best, underline is second best, † are zero-shot methods. N – number of hypotheses. *St.* stands for Steps.

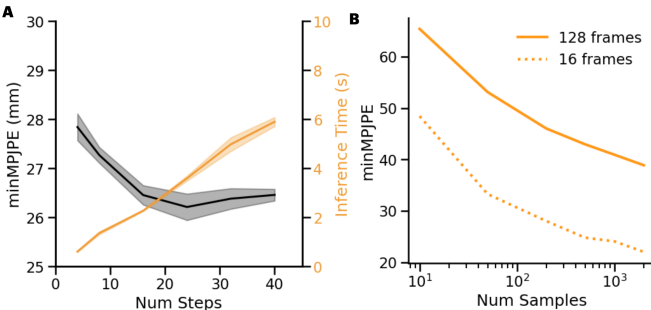


Fig. 5: **A)** Impact of the number of diffusion steps on minMPJPE and the inference time. Evaluated for single frame estimation. Mean and standard deviation are plotted from 3 seeds. **B)** Impact of the number of samples on minMPJPE for two different sequence lengths.

5.4 Ablation Study

Influence of inference steps We evaluate how the number of inference steps affects model performance. While the model was originally trained on 50 steps, we can change the number of steps and quantify the effect on performance and inference speed. In figure 5a we show the results of different numbers of inference steps. We evaluate on 1 frame long sequences, initiating sampling from 20% of the diffusion timesteps. For instance, with 8 inference steps, sampling starts from step 2 and progresses to step 10. We observe a slight perfor-

| Method | Sample Time (s) | Iterations |
|------------------|-----------------|------------|
| ZeDO | 11.0 | 1000 |
| Platypose | 1.1 | 8 |

Table 6: Time to generate 1 sample on GeForce 2080 Ti. **Bold** indicates best.

mance enhancement with increased steps, albeit at a notable expense in inference time.

Number of hypotheses We evaluate how changing the number of sampled hypotheses impacts joint error. As expected, increasing the number of hypotheses decreases the error. Longer sequences necessitate more samples for comparable performance to shorter ones. Sampling long sequences requires sampling from higher dimensional spaces. This is because more samples are needed to cover the same volume as for the short sequences. We show the results in figure 5b. Evaluation is conducted on every 10th example of the H36M test set using GT keypoints.

Influence of confidence Including the confidence of 2D keypoints should intuitively improve performance. In this ablation study we compare how 2D observation confidences affect performance. We test on 1 frames, with and without confidence estimates on H36M. We find that including confidence estimates helps decrease errors, but has no significant impact on calibration. Further improving the method of estimating the 2D confidence could lead to better performance.

| Confidence | minMPJPE | ECE |
|------------|---------------------|---------------------|
| ✓ | 46.4 45.6 | 0.02 0.02 |

Table 7: Impact of confidence on minMPJPE and calibration. Tested on 1 frame. **Bold** indicates best.

6 Limitations

Although Platypose demonstrates strong performance, it is not without limitations. We outline these limitations below. ① Like other zero-shot methods, Platypose relies on accurate camera parameters for estimating 3D poses. Additionally, it assumes prior knowledge of the root trajectory in 3D space. ② Platypose is not optimized for single hypothesis estimation. While it may not excel in this scenario, it is important to note that it is not its primary function. In the case of a well calibrated distribution, a single sample is not likely to fall close to the ground truth 3D pose. Thus, we would argue that a good performance of a multi-hypothesis method on one sample indicates an overconfident distribution. ③ There are instances where Platypose fails to generate reasonable 3D hypotheses. These failures may stem from issues with 2D keypoint detection or unexplained ambiguities. We include videos showcasing these failure examples in the supplementary materials.

7 Conclusions

In this paper we introduce Platypose, a zero-shot framework for estimating 3D human motion sequences from 2D observations. To the best of our knowledge we are the first to tackle the problem of multi-hypothesis motion estimation. We

condition a pretrained motion diffusion model using energy guidance to synthesize plausible 3D human motion sequences given 2D observations. We achieve state-of-the-art performance in comparison to baseline methods. Furthermore Platypose proves to be also capable of well-calibrated pose estimation.

Acknowledgments

We thank Arne Nix and John Peiffer for their helpful feedback and discussions. Funded by the German Federal Ministry for Economic Affairs and Climate Action (FKZ ZF4076506AW9) and SFB 1456 Mathematics of Experiment project number 432680300. RJC is supported by the Research Accelerator Program of the Shirley Ryan AbilityLab and the Restore Center P2C (NIH P2CHD101913).

References

1. Bar-Tal, O., Chefer, H., Tov, O., Herrmann, C., Paiss, R., Zada, S., Ephrat, A., Hur, J., Liu, G., Raj, A., Li, Y., Rubinstein, M., Michaeli, T., Wang, O., Sun, D., Dekel, T., Mossner, I.: Lumiere: A space-time diffusion model for video generation (2024)
2. Bridgeman, L., Volino, M., Guillemaut, J.Y., Hilton, A.: Multi-person 3d pose estimation and tracking in sports. In: 2019 IEEE/CVF Conference on Computer Vision and Pattern Recognition Workshops (CVPRW). pp. 2487–2496 (2019). <https://doi.org/10.1109/CVPRW.2019.00304>
3. Catalin Ionescu, Fuxin Li, C.S.: Latent structured models for human pose estimation. In: International Conference on Computer Vision (2011)
4. Chai, W., Jiang, Z., Hwang, J.N., Wang, G.: Global adaptation meets local generalization: Unsupervised domain adaptation for 3d human pose estimation. arXiv preprint arXiv:2303.16456 (2023)
5. Ci, H., Wu, M., Zhu, W., Ma, X., Dong, H., Zhong, F., Wang, Y.: GFPose: Learning 3D human pose prior with gradient fields (Dec 2022)
6. Dhariwal, P., Nichol, A.: Diffusion models beat GANs on image synthesis (May 2021)
7. Elfwing, S., Uchibe, E., Doya, K.: Sigmoid-weighted linear units for neural network function approximation in reinforcement learning (2017)
8. Gholami, M., Wandt, B., Rhodin, H., Ward, R., Wang, Z.J.: Adaptpose: Cross-dataset adaptation for 3d human pose estimation by learnable motion generation. In: Proceedings of the IEEE/CVF Conference on Computer Vision and Pattern Recognition (CVPR). pp. 13075–13085 (June 2022)
9. Gong, J., Foo, L.G., Fan, Z., Ke, Q., Rahmani, H., Liu, J.: Diffpose: Toward more reliable 3d pose estimation. In: Proceedings of the IEEE/CVF Conference on Computer Vision and Pattern Recognition (CVPR) (June 2023)
10. Gong, K., Zhang, J., Feng, J.: PoseAug: A differentiable pose augmentation framework for 3D human pose estimation. arXiv [cs.CV] (May 2021)
11. Gu, K., Chen, R., Yao, A.: On the calibration of human pose estimation (Nov 2023)
12. Guo, C., Mu, Y., Javed, M.G., Wang, S., Cheng, L.: Momask: Generative masked modeling of 3d human motions (2023)

13. Guo, C., Zou, S., Zuo, X., Wang, S., Ji, W., Li, X., Cheng, L.: Generating diverse and natural 3d human motions from text. In: Proceedings of the IEEE/CVF Conference on Computer Vision and Pattern Recognition (CVPR). pp. 5152–5161 (June 2022)
14. Ho, J., Jain, A., Abbeel, P.: Denoising diffusion probabilistic models. *Adv. Neural Inf. Process. Syst.* **33**, 6840–6851 (2020)
15. Ho, J., Salimans, T., Gritsenko, A., Chan, W., Norouzi, M., Fleet, D.J.: Video diffusion models (2022)
16. Holmquist, K., Wandt, B.: DiffPose: Multi-hypothesis human pose estimation using diffusion models (Nov 2022)
17. Ionescu, C., Papava, D., Olaru, V., Sminchisescu, C.: Human3.6m: Large scale datasets and predictive methods for 3d human sensing in natural environments. *IEEE Transactions on Pattern Analysis and Machine Intelligence* **36**(7), 1325–1339 (jul 2014)
18. Ji, H., Li, H.: 3D human pose analysis via diffusion synthesis (Jan 2024)
19. Jiang, Z., Ji, H., Menaker, S., Hwang, J.N.: Golfpose: Golf swing analyses with a monocular camera based human pose estimation. In: 2022 IEEE International Conference on Multimedia and Expo Workshops (ICMEW). pp. 1–6 (2022). <https://doi.org/10.1109/ICMEW56448.2022.9859415>
20. Jiang, Z., Zhou, Z., Li, L., Chai, W., Yang, C.Y., Hwang, J.N.: Back to optimization: Diffusion-based Zero-Shot 3D human pose estimation (Jul 2023)
21. Kanazawa, A., Black, M.J., Jacobs, D.W., Malik, J.: End-to-end recovery of human shape and pose (2018)
22. Kocabas, M., Athanasiou, N., Black, M.J.: Vibe: Video inference for human body pose and shape estimation. In: The IEEE Conference on Computer Vision and Pattern Recognition (CVPR) (June 2020)
23. Kocabas, M., Huang, C.H.P., Hilliges, O., Black, M.J.: PARE: Part attention regressor for 3D human body estimation. In: Proc. International Conference on Computer Vision (ICCV). pp. 11127–11137 (Oct 2021)
24. Kolotouros, N., Pavlakos, G., Jayaraman, D., Daniilidis, K.: Probabilistic modeling for human mesh recovery (Aug 2021)
25. Kumarapu, L., Mukherjee, P.: Animepose: Multi-person 3d pose estimation and animation. *Pattern Recognition Letters* **147**, 16–24 (2021). <https://doi.org/https://doi.org/10.1016/j.patrec.2021.03.028>, <https://www.sciencedirect.com/science/article/pii/S0167865521001215>
26. Li, C., Lee, G.H.: Generating multiple hypotheses for 3D human pose estimation with mixture density network (Apr 2019)
27. Loshchilov, I., Hutter, F.: Fixing weight decay regularization in adam. *CoRR* **abs/1711.05101** (2017), <http://arxiv.org/abs/1711.05101>
28. von Marcard, T., Henschel, R., Black, M., Rosenhahn, B., Pons-Moll, G.: Recovering accurate 3d human pose in the wild using imus and a moving camera. In: European Conference on Computer Vision (ECCV) (sep 2018)
29. Martinez, J., Hossain, R., Romero, J., Little, J.J.: A simple yet effective baseline for 3d human pose estimation (May 2017)
30. Mehta, D., Rhodin, H., Casas, D., Fua, P., Sotnychenko, O., Xu, W., Theobalt, C.: Monocular 3d human pose estimation in the wild using improved cnn supervision. In: 3D Vision (3DV), 2017 Fifth International Conference on. IEEE (2017). <https://doi.org/10.1109/3dv.2017.00064>, http://gvv.mpi-inf.mpg.de/3dhp_dataset

31. Müller, L., Osman, A.A.A., Tang, S., Huang, C.H.P., Black, M.J.: On self-contact and human pose. In: Proceedings IEEE/CVF Conf. on Computer Vision and Pattern Recognition (CVPR) (Jun 2021)
32. Oikarinen, T., Hannah, D., Kazerounian, S.: GraphMDN: Leveraging graph structure and deep learning to solve inverse problems. In: 2021 International Joint Conference on Neural Networks (IJCNN). pp. 1–9. IEEE (Jul 2021)
33. Oikarinen, T.P., Hannah, D.C., Kazerounian, S.: GraphMDN: Leveraging graph structure and deep learning to solve inverse problems. arXiv [cs.LG] (Oct 2020)
34. Pierzchlewicz, P.A., Cotton, R.J., Bashiri, M., Sinz, F.H.: Multi-hypothesis 3D human pose estimation metrics favor miscalibrated distributions (Oct 2022)
35. Pierzchlewicz, P.A., Willeke, K.F., Nix, A.F., Elumalai, P., Restivo, K., Shinn, T., Nealley, C., Rodriguez, G., Patel, S., Franke, K., Tolias, A.S., Sinz, F.H.: Energy guided diffusion for generating neurally exciting images (May 2023)
36. Raab, S., Leibovitch, I., Tevet, G., Arar, M., Bermano, A.H., Cohen-Or, D.: Single motion diffusion. In: The Twelfth International Conference on Learning Representations (ICLR) (2024)
37. Radford, A., Kim, J.W., Hallacy, C., Ramesh, A., Goh, G., Agarwal, S., Sastry, G., Askell, A., Mishkin, P., Clark, J., Krueger, G., Sutskever, I.: Learning transferable visual models from natural language supervision. In: International Conference on Machine Learning (2021), <https://api.semanticscholar.org/CorpusID:231591445>
38. Sharma, S., Varigonda, P.T., Bindal, P., Sharma, A., Jain, A.: Monocular 3D human pose estimation by generation and ordinal ranking (Apr 2019)
39. Sohl-Dickstein, J., Weiss, E.A., Maheswaranathan, N., Ganguli, S.: Deep unsupervised learning using nonequilibrium thermodynamics (Mar 2015)
40. Song, Y., Dhariwal, P., Chen, M., Sutskever, I.: Consistency models (Mar 2023)
41. Song, Y., Sohl-Dickstein, J., Kingma, D.P., Kumar, A., Ermon, S., Poole, B.: Score-based generative modeling through stochastic differential equations. In: International Conference on Learning Representations (2021), <https://openreview.net/forum?id=PxTIG12RRHS>
42. Soroush Mehraban, Vida Adeli, B.T.: Motionagformer: Enhancing 3d human pose estimation with a transformer-gcnformer network. In: Proceedings of the IEEE/CVF Winter Conference on Applications of Computer Vision (2024)
43. Tevet, G., Gordon, B., Hertz, A., Bermano, A.H., Cohen-Or, D.: Motionclip: Exposing human motion generation to clip space. In: Computer Vision–ECCV 2022: 17th European Conference, Tel Aviv, Israel, October 23–27, 2022, Proceedings, Part XXII. pp. 358–374. Springer (2022)
44. Tevet, G., Raab, S., Gordon, B., Shafir, Y., Cohen-Or, D., Bermano, A.H.: Human motion diffusion model (Sep 2022)
45. Vaswani, A., Shazeer, N., Parmar, N., Uszkoreit, J., Jones, L., Gomez, A.N., Kaiser, L., Polosukhin, I.: Attention is all you need (Jun 2017)
46. Wang, H., Su, B., Lu, L., Jung, S., Qing, L., Xie, Z., Xu, X.: Markerless gait analysis through a single camera and computer vision. Journal of Biomechanics **165**, 112027 (2024). <https://doi.org/https://doi.org/10.1016/j.jbiomech.2024.112027>, <https://www.sciencedirect.com/science/article/pii/S0021929024001040>
47. Wang, J., Lu, K., Xue, J.: Markerless body motion capturing for 3d character animation based on multi-view cameras (2022)
48. Wehrbein, T., Rudolph, M., Rosenhahn, B., Wandt, B.: Probabilistic monocular 3D human pose estimation with normalizing flows (Jul 2021)

49. Yoshida, H.: Construction of higher order symplectic integrators. *Physics Letters A* **150**(5), 262–268 (1990). [https://doi.org/https://doi.org/10.1016/0375-9601\(90\)90092-3](https://doi.org/https://doi.org/10.1016/0375-9601(90)90092-3), <https://www.sciencedirect.com/science/article/pii/0375960190900923>
50. Zheng, C., Zhu, S., Mendieta, M., Yang, T., Chen, C., Ding, Z.: 3d human pose estimation with spatial and temporal transformers. *Proceedings of the IEEE International Conference on Computer Vision (ICCV)* (2021)
51. Zhu, W., Ma, X., Liu, Z., Liu, L., Wu, W., Wang, Y.: Motionbert: A unified perspective on learning human motion representations. In: *Proceedings of the IEEE/CVF International Conference on Computer Vision* (2023)